Modeling Micro-Inclusion Growth and Separation in Gas-Stirred Ladles

Dong-Yuan Sheng*, Mats Söder**, Pär Jönsson**, and Lage Jonsson***

*MEFOS, SE-971 25 Luleå, Sweden.

**Division of Metallurgy, KTH, SE-100 44 Stockholm.

***MEFOS. Also, a Prof. at KTH.

ABSTRACT

Mathematical models of inclusion behavior in stirred ladles are useful for both increasing our fundamental understanding of the growth and removal of inclusions as well as for future use in process control. This study reports on some efforts to use both static and dynamic modeling to better understand inclusion behavior in gas-stirred ladles. A computational-fluid-dynamics mathematical model of a gas-stirred ladle was developed earlier. In the investigation covered in this report, instantaneous fluid-flow results from the model were used in combination with inclusion growth and removal theories in order to study the importance of bubbles on inclusion flotation. The study results proved to be highly dependent on the theory used to describe bubble flotation. The model of the gas-stirred ladle was also used together with the inclusion theories to study the transient behavior of inclusions during growth and removal. The dynamic simulation results indicated that inclusion concentration gradients exist. The most important research task in the near future is to verify static and dynamic modeling results of inclusion behavior during stirring with experimental data. Here, the authors feel that carefully performed plant trials could provide useful information.

1 INTRODUCTION

There is a need for mathematical models that can predict the growth and separation of micro-inclusions in stirred ladles. The reason is that today it is not possible to control the micro-inclusion characteristics during ladle refining using traditional methods. This is more obvious if one studies the example in **Table I**. Here the three quality parameters that are used for control in the production of "clean steel" are compared throughout the process. The first parameter is elements dissolved in the liquid steel. These are relatively simple to determine by taking a ladle, tundish or mold sample followed by chemical analysis. Usually, an analysis can be ready within 7 to 10 minutes from sampling. Thus, the operator has a chance to make adjustments during liquid steel treatment in the ladle. After the steel is solidified the chemical composition does not usually change much and further process control is unnecessary. The second quality parameter is temperature. This can easily be determined rapidly during liquid steel treatment and metalworking. Thus, temperature can also be controlled throughout the process. The third quality parameter pertains to inclusions characteristics. Inclusions are normally categorized as micro-inclusions (here defined as smaller than 22 μm) and macro-inclusions (>22 μm). For the majority of steel companies, a means of rapid feedback of inclusion characteristics during liquid steel making is not available and steel cleanness can therefore not be controlled the with respect to inclusion content. One company, Ovako Steel AB, has reported[1,2] that they are currently testing a modified OES (optical emission spectroscopy) method that they have developed for on-line determination of micro-inclusion size distribution.

It is clear that there is a need for mathematical models that can provide useful information regarding the growth and separation of non-metallic inclusions for companies lacking on-line determination of inclusion characteristics. Even for a company like Ovako Steel, mathematical models of micro-inclusion behavior are useful during that period (7 to 10 minutes) when the operator is waiting for the analysis results or during vacuum degassing, when sampling is not possible.

In the following paper, modeling inclusion growth and separation during gas stirring of the ladle is discussed. Results from using both a static and dynamic approaches are presented. The first part of the paper describes the earlier efforts made to model inclusion growth and

separation using computational fluid dynamics (CFD) to calculate the fluid-flow and heat-transfer characteristics with fundamental transport equations. The next sections cover the most relevant theories accounting for inclusion growth and removal, the static and dynamic modeling, and finally, presentation and discussion of the investigation results.

2 PREVIOUS MODELING OF INCLUSION GROWTH AND REMOVAL

Many researchers have studied the growth and removal of inclusions. Some of the pioneers in the field of mathematical modeling of the process are Lindborg and Torsell[3]. In 1968 Lindborg and Torsell presented a model of inclusion growth and removal relevant for laboratory study. A population balance considering Stokes and turbulent collisions and removal by Stokes flotation was used. Later, stirring by natural convection and removal by flotation was studied by Iyengar and Philbrook[4]. The separation of inclusions to the refractory wall was investigated by Linder[5]. He studied the effect of different parameters on the population balance. The removal of inclusions to the refractory wall was also modeled by Engh and Lindborg[6].

In the mid 1970s fluid modeling started to be used for calculating the growth and removal of inclusions. **Table II** lists the published studies that used fundamental transport equations. One of the first published articles are by Nakanishi and Szekely[7]. A population balance equation was used and turbulent collisions were taken into account using an expression suggested by Saffman and Turner[8]. Using the average energy dissipation from a mathematical fluid model of a 50-tonne ASEA-SKF ladle, they calculated the deoxidation kinetics and compared the results with experimental data from a production ladle. The discrepancy between the calculated and the experimental data were handled by introducing a coagulation coefficient ranging between 0.27-0.63 in their experiments. Later, Shirabe and Szekely[9] made a fluid-flow model including turbulence with an inclusion coalescence model for a R-H vacuum degasser. Navier-Stoke's equations were used in combination with the well-known k-ε model to model the turbulent flow. The spatial size distributions of the inclusions were presented in the results. In 1986, Johansen, Boysan and Engh[10] also modeled the fluid flow in steel and inclusion behavior in a similar manner as Shirabe and Szekely, but for a gas-stirred ladle. In addition, they modeled the gas phase using a Lagrangian approach.

They also took the separation of inclusions to the slag and refractory and the dissolution of the refractory into account.

Today, three-dimensional models have become more common. A number of 3-D models for tundishes have been developed using the k-ε model to take turbulence into account and more or less complex models to describe inclusion growth and removal[11-16]. In the late 1990s some more comprehensive models were made. In 1997 Miki et al.[17] presented a model of inclusion removal in a R-H vacuum degasser. They considered the effect of argon using a volume-fraction-of-fluid model. However, they used the average value of the energy dissipation when calculating the growth and separation of inclusions. With a simple model, the removal of inclusions due to gas bubble flotation was also considered. Miki et al.'s model also included the flotation of clusters in addition to single inclusions. Cluster formation was likewise considered by Wakoh et al.[18], Tozawa et al.[19] and Miki and Thomas[20]. In addition, Wakoh et al. also considered slag dispersion into the steel.

3 INCLUSION THEORIES

3.1 Growth of Inclusions

Immediately after the aluminum has been added to the steel, it rapidly reacts with oxygen to form alumina inclusions. Initially the total oxygen content in the molten steel is still high since the oxygen is still present in the steel in the alumina inclusions. As the number of inclusions is large, the probability of collision is also quite high. Therefore, stirring can promote inclusion collision and agglomeration. The number of collisions due to certain phenomena can be calculated in the general form as:

$$\frac{dn_{i,j}}{dt} = \sum W_{ij} n_i n_j \qquad (1)$$

where $W_{i,j}$ = collision volume, m^3/s

n_i, n_j = number of inclusions of size i and j, $1/m^3$

The collision volume, W_{ij}, represents a rate factor for the collisions of a certain growth mechanism and has the unit m^3/s (thus the name).

The following mechanisms are believed to influence inclusion growth:

1. Diffusion of oxygen and deoxidant to the surface of the inclusion
2. Diffusion coalescence, so-called Ostwald ripening
3. Collision due to Brownian motion
4. Collision due to velocity gradients in laminar shear zones
5. Collision due to turbulence
6. Collision due to buoyancy differences, so-called Stoke's collisions

In general, the first four mechanisms are not considered to be so significant. In the literature, growth due to turbulent collisions is often suggested as the most important mechanism[3,5,7,9,12,14,16,17,22,23]. Small eddies in the turbulent fluid are believed to cause collisions between the inclusions. The collision volume for turbulent collisions can be described according to an equation formulated by Saffman and Turner[8] which has been modified to the following form[7,22,24]:

$$W_{ij} = 1.3\pi^{1/2}\alpha\left(r_i + r_j\right)^3\sqrt{\frac{\varepsilon}{\nu_{Fe}}} \qquad (2)$$

where α = collisions efficiency

$r_{i,j}$ = inclusion radius, m

ε = turbulent energy dissipation, m^2/s^3

ν_{Fe} = kinematic viscosity, m^2/s

The sixth mechanism, growth due to difference in buoyancy, is also thought to be of importance in some cases. Inclusion growth generated by this mechanism is due to the fact that the velocity difference between inclusions makes larger inclusions catch up with smaller ones. The collision volume for Stoke's collisions can be expressed as[3]:

$$W_{ij} = \frac{2\pi g\left(\rho_{Fe} - \rho_i\right)}{9\mu_{Fe}}\left(r_i + r_j\right)^3\left|r_i - r_j\right| \qquad (3)$$

where g = gravitational constant, m/s^2

ρ_{Fe} = steel density, kg/m^3

ρ_i = inclusion density, kg/m^3

μ_{Fe} = steel viscosity, kg/sm

In the section on dynamic modeling, collision by Brownian motion is formulated. The collision volume is calculated[24] as

$$W_{ij} = \frac{2kT}{3\mu_{Fe}}\left(\frac{1}{r_i}+\frac{1}{r_j}\right)\left(r_i + r_j\right) \quad (4)$$

where k = the Boltzmann constant, J/K

T = Temperature, K

3.2 Removal of Inclusions

There are three ways by which inclusions can leave the gas-stirred melt: (i) by floating out and being absorbed by the top slag, (ii) by sticking to the refractory wall, and (iii) by bubble flotation and being absorbed by the top slag.

3.2.1 Removal to the Top Slag

The rate of removal to the top slag is controlled by the number of inclusions in the region under the slag/steel interface and the size of those inclusions. As the size increases the buoyancy increases to the second power. Larger inclusions are therefore more readily removed. A removal equation in accordance with Stokes law can be expressed in the following way:

$$\frac{dN}{dt} = A_s \cdot \frac{2g(\rho_{Fe} - \rho_i)r^2}{9\mu_{Fe}} \cdot C_i \quad (5)$$

where A_s = slag area, m^3

C_i = inclusion concentration, 1/m^3

3.2.2 Removal to the Refractory

Inclusions can be removed to the refractory by the motion of the steel. In the literature, the removal is considered to be controlled by turbulent diffusion to the refractory surface. It can, for example, be modeled as suggested by Linder[5]:

$$\frac{dN}{dt} = A_w \cdot \frac{0.0003 \cdot r_i \overline{U}^{7/4}}{\upsilon^{3/4} d^{1/4}} \cdot C_i \qquad (6)$$

where A_w = refractory area, m3

$\overline{U}$ = fluid velocity, m/s

d = "tube diameter", m

The value of d was somewhat arbitrarily given the value of 0.01. The equation is not very dependent on the value of d since it is raised to the power of ¼ in equation (6).

3.2.3 Removal by Bubble Flotation

When the ladle or any other metallurgical vessel is stirred by inert gas bubbling, there is a chance that inclusions will attach to bubbles and be lifted to the surface. The alumina inclusion has a large contact angle with steel, ~140°, which suppresses wetting between steel and alumina, and increases its chances of attaching to a gas bubble that is rising in the steel.

Three models for the description of flotation of inclusions by bubbles have been published. Often the inspiration behind these theories has come from the field of mineral processing, where bubble flotation is widely used. Below, a brief description of the models is given.

Flotation model 1

Wang, Lee and Hayes[25] proposed a model for the removal of inclusions by gas bubbles. The work is in turn based on work by Yoon and Lutrell[26]. The probability for the coalescence of an inclusion and a gas bubble is calculated based on a stream function, a submechanism for the sliding over the bubble surface, and the final rupture of the film around it. The overall probability is formulated as:

$$P = P_c P_a \tag{7}$$

where P_c = probability of collision

P_a = probability of attachment

All collisions do not lead to a formation of an aggregate. In order for a successful collision to occur, the inclusion has to make contact with the gas. During this process the inclusion slides over the bubble surface. As the thin film between the gas and the inclusion gets thinner it eventually ruptures and contact is achieved. This process only occurs if the sliding time is longer than the rupture time for the film. Therefore, a separate equation for the probability of attachment needs to be solved. This in turn requires that additional equations be solved for the sliding and collision times . Two cases for the bubble-film rupture are calculated here: Model 1a and Model 1b[25,27]. In the end, the final removal equation due to bubble flotation in the probability model can be formulated as:

$$\frac{dN}{dt} = PN_b v_r \pi \left(r_b + r_i\right)^2 C_i \tag{8}$$

where N_b = number of bubbles, $1/m^3$

v_r = relative velocity between steel and gas, m/s

r_b = bubble radius, m

Flotation model 2

In an article by Miki et al.[17] inclusion removal by bubble flotation was calculated based on a common stream function for potential flow around the bubble. From the stream function a critical inclusion entrapment radius was calculated. In the Miki et al. model, an expression of collision efficiency based on work by Frisvold et al.[28] was incorporated. The collision efficiency takes the boundary layer between the bubble and the inclusion into account. The final removal equation can be expressed as:

$$\frac{dN}{dt} = \frac{1}{2}\frac{r_i}{r_b}\sqrt{\frac{3}{2}\mathrm{Re}_b} \cdot C_i N_b v_r b^2 \pi \tag{9}$$

where Re_b = Reynolds number for bubbles

b = critical entrapment radius, m

Flotation model 3

Prior to Miki et al.[17], Engh[29] used the same stream function to derive a simple bubble flotation equation. The removal function is formulated as:

$$\frac{dN}{dt} = 3 r_i v_r \pi r_b C_i N_b \qquad (10)$$

4 MATHEMATICAL MODELING

Modeling the growth and separation of inclusions in stirred ladles is a task that requires a multidisciplinary and extensive research. In the authors' opinion, it is very hard to create an inclusion model based on fundamental transport equations that can be used to follow the inclusions throughout the entire ladle refining process. Therefore, the modeling work in this paper has been confined to describing the part of the process where the final deoxidation, using aluminum, takes place. The aluminum deoxidant was assumed to be fed to the steel using wire injection. It then melts and reacts with the oxygen, which results in the nucleation of solid alumina inclusions. The nucleation was not considered. Instead the modeling focused on the growth and separation of the alumina inclusions during a 5-minute period of constant stirring using argon gas (80 l/min.) at atmospheric pressure above the melt. The initial size distribution of the inclusions used in the simulations was taken from analysis data of samples taken in liquid steel.

4.1 Mathematical Model of Fluid Flow in a Gas-Stirred Ladle

A two-dimensional two-phase model of a gas-stirred ladle was developed earlier [30,31]. In this study, the model was used to model a ladle having a 1.40 m radius and a steel-bath height of 2.35 m. An argon flow of 80 l/min was used. The gas is injected through a centrally placed nozzle in the bottom of the ladle. A sketch of the gas-stirred ladle is given in **Figure 1**. Below, the assumptions made and the general transport equations are specified. Details regarding the fluid-flow model assumptions, transport equations, boundary conditions, property variations, turbulence model, interface friction forces, etc. can be found in a previous publication[31].

Assumptions

The following assumptions are made in the statement of the mathematical model:

(a) The gas-stirred ladle is axially symmetric, so the governing equations can be written in two-dimensional cylindrical coordinates. Velocities and volume fractions are predicted for both the liquid and the gas phase over the whole domain based on Eulerian equations.

(b) The calculations are performed using the transient solution mode.

(c) A two-fluid version of the k-ε two-equation model is used to describe the turbulence in the liquid steel[32].

(d) The free surface is flat, but an allowance is made for the escape of gas bubbles at the surface.

(e) The gas bubbles are introduced through a nozzle located in the center of the ladle bottom.

(f) An interface friction coefficient is used to describe the force between the gas and liquid phases.

Transport Equations

According to the above assumptions, the following general governing transport equation need to be solved:

$$\frac{\partial(\alpha_i\rho_i\varphi_i)}{\partial t} + div(\alpha_i\rho_i v_i\varphi_i - \alpha_i\Gamma_{\varphi i} grad\varphi_i) = \alpha_i S_{\varphi i} \qquad (11)$$

where α_i = volume fraction of phase i ;

ρ_i = density of phase i

φ = variables solved (u, v, w, k, ε)

$\Gamma_{\varphi i}$ = effective diffusion coefficient

$S_{\varphi i}$ = source terms

Equation (11) is used to represent all conservation equations by setting $\Gamma_{\varphi i}$ and $S_{\varphi i}$ to appropriate values according to the dependent variable φ_i.

4.2 Inclusion Model

The following sections contain more detailed information on the assumptions, initial conditions, boundary conditions, source terms, and the method of solution for the inclusion model.

4.2.1 Assumptions

The following assumptions are made in the statement of the current inclusion model:

a) The transient inclusion concentration equations are solved based on the steady state flow pattern. This means that the movement of particles in the molten steel is assumed not to affect the fluid flow. This is acceptable since the inclusion size considered in this study is lower than 22 μm and the inclusion fraction is also very low.

b) The generation of inclusions in the gas-stirred ladle due to erosion of refractory, entrapment of slag and chemical reactions is not considered.

c) The inclusions are assumed to be spherical particles with the density[16] of 3260 kg/m^3. This is representative of Al_2O_3 particles in the steel. The initial size is based on production sample analyses.

d) Inclusion collision is assumed to occur between two spherical particles forming a bigger spherical inclusion. Cluster formation due to collisions between several particles is not considered.

e) The attachment of inclusions to argon bubbles is calculated under the assumption that inclusions' center lines flow along streamlines and attachment of an inclusion to a bubble occurs when a streamline carrying an inclusion comes closer to the bubble than the length of the inclusion's radius. This is a simplification used as a first attempt to model bubble flotation of inclusions.

f) An inclusion is separated to the refractory when it is within the laminar boundary layer near the wall. When this occurs, it is removed from the system (from a computational viewpoint).

g) The free surface is flat and slag layer is not taken into account. Ideal absorption by the slag is therefore assumed in the specification of the boundary condition pertaining to inclusions at the top free surface.

4.2.2 Equations

The distribution of the weight concentration of the inclusion particles is calculated using a scalar variable (*C)*. It is determined with the following equations based on the given flow pattern calculated previously.

$$\frac{\partial(\alpha_l \rho_l C_{ln})}{\partial t} + div(\alpha_l \rho_l v_p C_{ln} - \alpha_l \Gamma_{C_{ln}} grad C_{ln}) = \alpha_l S_{C_{ln}} \quad (12)$$

where α_l = volume fraction of liquid phase

ρ_l = density of liquid phase

C_{ln} = weight concentration of inclusions belonging to different size groups

$\Gamma_{C_{ln}}$ = effective diffusion coefficient of the inclusions

$S_{C_{ln}}$ = source terms of growth and removal

The effective diffusion coefficient $\Gamma_{C_{ln}}$ is the sum of two components:

$$\Gamma_{C_{ln}} = \frac{\mu_l}{Sc_l} + \frac{\mu_t}{Sc_t} \quad (13)$$

where μ_l , μ_t = laminar and turbulent viscosity of liquid, respectively

S_{C_l} , S_{C_t} = laminar and turbulent Schmidt number, respectively

The inclusion is subject to the laminar and turbulent dispersion with the Schmidt number equal to one.

In this study the inclusions are divided into three groups based on the experimental information given in **Table 3**. This means three similar additional concentration transport equations (equation 12) are solved. Each has different initial concentration values, boundary conditions and source terms.

In equation (12), the particle velocity is expressed as $v_P = (v_r, v_z + v_{st})$, where v_r and v_z are the radial and axial velocities. The Stoke's velocity of the inclusion (v_{st}) is taken as an extra convective component, calculated from the following equation:

$$v_{st} = g(\rho_i - \rho_p) D_p^2 / 18 \mu_l \quad (14)$$

The transient inclusion weight fraction is defined as:

$$\eta = G_t^{t^*} / G_t^0 \quad (15)$$

where the initial inclusion weight is G_t^0, and the inclusion weight at a certain time point is $G_t^{t^*}$. Hence, the sum initial weight fractions (η) of each of the three different inclusion groups is equal to 100%.

4.2.3 Growth and Removal Equations

Initial conditions

All the solved and stored variables calculated from the fluid-flow model were used as input when modeling the dynamic inclusion behavior. The initial concentrations of inclusions were taken from an analysis of a production sample. The size distribution was determined using an optical microscope and the inclusions were classified by the Swedish standard SS 11 11 16 (JK chart II)[21]. In accordance with this standard, inclusions found in samples taken in liquid steel are classified as undeformed, or D-type, inclusions. Inclusions are also further divided into four groups according to width/diameter: i.e. thin (DT), medium (DM), heavy (DH) and particular (DP). The first three inclusion groups are typically found in clean steel. The first three size groups are defined and the initial conditions used in are specified in **Table 3**.

Inclusion growth

The inclusion growth due to collision is described using the following source term:

$$Sc = \rho_p V_p (W_{ij}^1 + W_{ij}^2 + W_{ij}^3) \cdot n_i \cdot n_j \cdot dr \cdot d\theta \cdot dz \cdot dt \qquad (16)$$

where W_{ij}^1 is the Brownian collision volume (equation 4), W_{ij}^2 is the Stoke's collision volume (equation 3), and W_{ij}^3 is the turbulence collision volume (equation 2).

Inclusion separation to the surface

The separation of inclusion particles to the top surface is expressed as a boundary condition:

$$q_s = v_{st} C_{ln} \qquad (17)$$

where q_s and C_{ln} are the upward inclusion flux density and the inclusion concentration at the surface, respectively. The inclusion outgoing flux is different for the three different groups of inclusions due to different Stoke's velocities (v_{st}).

Inclusion separation to the wall

The separation of inclusion particles to the ladle refractory wall is expressed as boundary conditions in the following manner. According to the log-law wall function [33], the laminar boundary layer is calculated by the dimensionless distance from the wall, y^+:

$$y^+ = \frac{y_w C_\mu^{0.25} k^{0.5}}{\nu_l} \tag{18}$$

If the y^+ value in the grid near the wall is lower than 11.63, all inclusions in the cell are considered to be removed from the system. If the y^+ value in the grid is higher than 11.63, the thickness of the laminar boundary layer is first calculated as follows [14]:

$$\delta = \frac{10\nu_l}{C_\mu^{0.25} k^{0.5}} \tag{19}$$

Thereafter, the weight fraction of the inclusions in the cell which are separated to the wall is calculated as:

$$\eta_w = 1 - \delta / y_w \tag{20}$$

Inclusion separation due to bubble flotation

The separation of inclusions due to bubble attachment is described using a source term. According to Engh [29], the volume of inclusion bubble attachment can be estimated as follows:

$$W_b = \eta_b \cdot v_b \cdot \pi \cdot r_b^2 = \frac{3r_p}{r_b} \cdot v_r \cdot \pi \cdot r_b^2 \tag{21}$$

The source term for bubble attachment can then be expressed as:

$$Sc = \rho_p V_p W_b \cdot n_b \cdot n_i \cdot dr \cdot d\theta \cdot dz \cdot dt \tag{22}$$

4.3 Method of Solution

4.3.1 Fluid-Flow Simulation

For the fluid-flow model, the solutions of the governing equations, boundary conditions, and source terms were obtained using the general CFD software package PHOENICS 3.1. The algorithm IPSA is used to solve two-phase fluid-flow problems[34,35]. A typical calculation used 20,000 sweeps for a 30 × 41 non-uniform mesh and required 2.5 hours of CPU time on a SUN workstation.

4.3.2 Static Simulation of Inclusion Growth and Removal

In the static modeling, the output from a simulation of the fluid flow in a gas-stirred ladle was used (model described in section 4.1). The data obtained from the CFD simulation includes velocity, dissipation of turbulent kinetic energy, fraction of gas, etc. This data was used as input to models of different theorized mechanisms of inclusion growth and separation.

4.3.3 Dynamic Simulation of Inclusion Growth and Removal

The FORTRAN source code developed to calculate the growth and separation of inclusions described in section 4.2 was incorporated into the user interface of PHOENICS as an additional subroutine. The time step of transient inclusion simulation was set to one second and the iteration set to 200 sweeps per time step. The output data was saved in a file every ten seconds. Thus, the simulated five minutes of inclusion growth and removal during gas stirring required 8 hours of CPU time on a SUN workstation. The flow chart of the simulation is shown in **Figure 2**.

5 RESULTS

All the modeling results presented in this section correspond to the conditions specified in section 4. Results from the fluid-flow modeling are presented first, followed by sections on results from the static and dynamic modeling. A final discussion of the total influence on inclusion modeling using results from both approaches concludes the overall section on the study's results

5.1 Fluid Flow

A two-dimensional mathematical model of a gas-stirred ladle was used, where argon gas is injected through a centrally placed nozzle. The argon flow was 80 l/min for all predictions shown in section 5.

The fluid-flow pattern at the central plane of the ladle is shown in **Figure 3a**, illustrated with vectors. The buoyancy force resulting from the injection of argon gas gives rise to high steel velocities at the center of the ladle. Thereafter, the steel is directed towards the ladle wall and then downwards along the side wall. As a result, a large clockwise circulation loop is created in the steel bulk. The gas fraction and turbulent energy dissipation rate results are shown in **Figures 3b and 3c**. The fraction of gas is highest in the center of the ladle, which is expected since the gas is injected in this region. Some gas can also be seen to have spread in the radial direction to the upper part of the ladle, carried by the radial steel flow. The dissipation of the kinetic energy is highest where the velocity vector values are highest, close to the gas plume and parallel to the slag/metal interface.

5.2 Static Modeling Results

The fluid-flow and turbulence data from the two-dimensional CFD model of a gas-stirred ladle were used as input in making the instantaneous calculations of inclusion growth and separation. In order to compare the two most important collision-growth mechanisms, the collision volume was calculated for turbulent and Stoke's collisions. The turbulent-collision volume was calculated using a weighted average value of the energy dissipation for the gas-stirred ladle. The calculation results are presented in **Figure 4**. The figure illustrates how the collision volume for an inclusion of 2μm changes when it collides with inclusions of different radius lengths. As can be seen, turbulent collision is the most important micro-inclusion growth phenomenon for the gas-stirred ladle during the stirring period. It can also be seen that when the difference in size between inclusions is large, the Stoke´s collision mechanism becomes more important. It is possible that Stoke's collisions would even be more important if inclusions larger than 22 μm were considered. However, that issue was not within the scope of this work.

It can also be seen in **Figure 4** that the collision volume increases with an increased size in the colliding inclusion. However, the total number of collisions is also a function of the number of inclusions of different sizes. **Table 3** illustrates that the number of larger inclusions (DH) is much lower than the number of smaller inclusions (DT and DM). Therefore, the number of collisions for large inclusions is still lower than that of small inclusions.

The static modeling approach was also used to compare the separation of inclusions due to different mechanisms. In **figure 5**, the inclusion removal rate is plotted as a function of inclusion size. Removal by the different mechanisms described in section 3 was predicted for the whole ladle. For each case, a summation of the removed fractions of all cells used in the CFD calculation of fluid flow in the gas-stirred ladle was made. A general trend illustrated in **Figure 5** is that the inclusion removal rate due to all mechanisms increases with an increased inclusion size. The highest removal rates correspond to separation to the slag by Stoke's flotation and to the refractory wall. Separation to the refractory bottom and by bubble attachment and then separation to the slag seem to be of less importance.

It is also interesting to note that very different results were obtained for the three models expressing the flotation of inclusions due to bubble attachment (**Figure 5**). The use of models 1a and 1b resulted in the lowest removal rate predictions. Models 1a and 1b used expressions for the film-rupture time and the film-drainage time, respectively, to determine when a gas bubble and an inclusion come in contact with each other. The two approaches rendered very similar results. However, the removal rates for models 2 and 3 were considerably higher than for models 1a and 1b. One reason for this is in the theory applied in expressing inclusion bubble attachment[25,27]. In models 1a and 1b, the assumption of point contact between the bubble and the inclusion was used to determine when attachment occurs. In models 2 and 3, an assumption of plane contact was used, which increases the probability of attachment of inclusions to bubbles. The two contact mechanisms represent two extreme cases. In reality, bubbles are much larger than micro-inclusions, so the actual contact geometry should be closer to plane contact than point contact.

Another reason why the results from models 1a and 1b differ from those from models 2 and 3 is that different assumptions of the flow conditions are used in the models. In models 1a and 1b the collision probability is calculated using an expression valid for Reynolds numbers for gas bubbles of intermediate values (1 to 500). In models 2 and 3, the fluid flow is assumed to represent Reynolds numbers in the order of several thousand. Output from the CFD model of the gas-stirred ladle shows that Reynolds numbers for bubbles are closer to the assumptions used in models 2 and 3 than models 1a and 1b.

In models 2 and 3, the same assumptions are made regarding the fluid flow, but still the results differ. The difference can be explained in the way the critical entrapment radius, b, is

calculated in the two models. The distance at which *b* is calculated in model 2 is defined to be close to the bubble. In model 3, the entrapment radius is defined as being at a distance farther away from the bubble. Thus, the entrapment radius will be larger, which will result in a higher removal rate in comparison to the predictions using model 3.

5.3 Dynamic Modeling

Results from the dynamic simulations of inclusion behavior are presented in **Figure 6**. The figure shows the contour plots of particle densities. The results represent a typical simulation case where all growth and removal mechanisms specified in section 3 are taken into account. In comparing the three different groups in **Figure 6**, it can be seen that the particle density in the steel decreases with increasing particle size. The initial value of the particle density is $2.3*10^{10}$ l/m^3 for the smallest (DT type) inclusions (**Figure 6a**). After 1 minute of stirring, the inclusion density in the plume region has decreased substantially. A similar tendency can be seen for the larger inclusion sizes (DM and DH) in **Figures 6b and 6c**. There are some explanations for the lower inclusion density in the plume region: i) a high turbulence energy dissipation increases the probability of turbulent collision, ii) a high gas fraction increases the probability of inclusions attachment to bubbles and transport to the slag where they are separated, and iii) clean steel is fed to the nozzle region by the circulation loop. In the last case, the steel flows parallel to the slag, downwards along the wall, parallel with the bottom, and finally up again to the plume region. Inclusions therefore are more likely to be separated to the slag and refractory, which results in the steel in the plume region containing fewer inclusions.

In order to compare the different mechanisms of inclusion growth and removal, a sequence of simulations was done, where one individual mechanism was considered in each simulation. In **Figure 7a** , the results pertaining to the turbulent-growth simulation are illustrated. The weight fraction of smallest particles (Group C, 2.8-5.6μm) decreases about 10% after 5 minutes of gas stirring. The disappearance of the smaller size particles creates new particles of larger size, which gives a supply of new inclusions to Group B. Group B also loses inclusions due to its own collision growth. This causes the weight of the fraction of DM size particles (Group B, 5.6-11.2 μm) to stay almost the same during the 5-minute stirring period. A similar tendency can be seen for the DH size inclusions.

Figure 7b shows the simulation results for when only bubble attachment was taken into account. It can be seen that the DH inclusions will decrease about 18% while the DT inclusions only decrease about 3% during the 5-minute stirring period. This indicates that the large inclusions are more easily removed by attachment to gas bubbles.

Figure 7c shows the change of inclusion weight fraction calculated only considering the wall attachment. The removal of inclusions occurs at the same rate for all three groups and corresponds to about a 10% decrease during the 5 minute treatment. The results indicate that the inclusion attachment to the refractory is also an important mechanism that can not be neglected.

Figure 7d shows the change in the inclusion weight fraction for the simulation considering only ideal absorption of inclusions by the top slag. The difference among the three inclusion size groups is clear. About 37% of the largest inclusions are removed during the 5-minute treatment period, mainly due to high upwardly directed Stoke's velocities. Compared to the other removal mechanisms, removal to the top slag is the most important for the largest inclusions. However, removal due to slag absorption does not seem to be very significant for smaller inclusions.

Figure 8 shows the weight fractions for the different simulations of inclusion growth and removal after 5 minutes of stirring. It can be seen that turbulent collision and wall attachment are the most important factors influencing the growth and removal of small inclusions. Bubble attachment and absorption by the slag are more effective in removing larger size particles. Also, the amount of growth due to Brownian motion and the Stoke's collision mechanism is relatively minor. Finally, the largest inclusions are seen to be more easily removed than the smaller.

From **Figure 8C**, the removed weight fraction of the largest inclusions due to the different growth and removal mechanisms are as follows: 1) Brownian motion, 0.2%; 2) Stoke's collision, 1%; 3) turbulent collision, increase 1%; 4) bubble attachment, 19%; 5) slag absorption, 37%; 6) wall attachment, 10%. The total removal fraction is 47%. Note here that the total fraction removed is not equal to the sum of the individual mechanisms' weight fractions removed. This is due to the fact that the calculated local inclusion concentration is

not only determined by the growth and removal source term, but also the fluid-flow diffusion and convection terms.

5.4 Discussion

In this paper examples of using both static and dynamic modeling to study the growth and removal of inclusions in gas-stirred ladles were given. First, static modeling was used to compare different mechanisms suggested to explain the separation of inclusions by bubble attachment. In this part of the study highly different case results were obtained based on the assumptions made in the different equations describing the separation of inclusions by bubble attachment. This illustrates the usefulness of static modeling to select the theories which best describe the situation modeled. Thereafter, dynamic modeling can be carried out to study the transient situation. This will save time, since dynamic modeling is more time consuming than static modeling.

6 CONCLUSIONS

The growth and the separation of alumina micro-inclusions were studied using both static and dynamic modeling. The study focused on a 5-minute period of gas stirring carried out after the final deoxidation in the ladle. The nucleation of inclusions was neglected. Instead, the initial micro-inclusion size distribution used in the model was taken from experimental data. A CFD model of a gas-stirred ladle was used to calculate fluid flow and turbulence data. In the static modeling effort, the output from the CFD simulations was used in equations expressing the growth and removal of micro-inclusions. Results from the static model showed that micro-inclusion growth mainly takes place as a result of turbulent collisions, which is in agreement with previously published results[3,5,7,9,12,14,16,17,22,23]. The results also showed that collisions due to buoyancy becomes important when the difference in inclusion radius becomes larger than approximately 10 microns. The importance of the Stoke's collision mechanism for inclusions differing significantly in size has also been noted by other researchers[16-20]. The static modeling results illustrated that the predicted removal of micro-inclusions due to bubble flotation is highly dependent on the flotation theory employed.

In the dynamic modeling effort, theoretical expressions of inclusion growth and removal were incorporated into the CFD model of the gas-stirred ladle. The main conclusion drawn from the results of this part of the study is that concentration gradients of inclusions exist. After 1 minute of gas stirring, regions with fewer inclusions were found close to the gas plume and the slag/steel interface. This is probably due to inclusion growth by turbulent collision caused by high values of the dissipation of kinetic energy and separation to the top slag and refractory. The inclusion population in the bulk of the ladle decreased very slowly due to little turbulent-collision growth in this low-turbulence region. Furthermore, the separation of inclusions was limited by slow transport of the steel to the slag and refractory. Based on the governing conditions upon which the dynamic modeling was done, the following conclusions were also drawn.

- The particle number density decreases with an increasing particle size.
- The largest inclusions (DH) are more easily separated from the steel to the slag due to both the Stoke's mechanism and bubble flotation.
- The rate of separation of inclusions to the wall is same for all sizes of inclusions.
- The transient simulation showed that the total inclusion fraction removed is not equal to the sum of the individually calculated fractions corresponding to the influence of the different mechanisms. This is because the inclusion concentration changes not only as a result of growth and removal, but is also influenced by fluid flow characteristics.

Finally, it must be stated that verification of the model results by comparison with corresponding plant trial results is highly desirable. It is necessary to verify the existence of concentration gradients of different inclusion populations in the ladle during different stirring conditions. Such verification is possible provided that sampling can be done at different locations simultaneously. Also, advanced techniques such as the OES method could be used for rapid feedback on inclusion characteristics. Thereafter, if the model predictions were to agree reasonably well with the trial data, the development of simpler control models based on fundamental mathematical models and advanced analysis techniques could be initiated.

In the future, parameter studies focusing on, for example, i) the most suitable equations for modeling bubble flotation, ii) influence of the turbulence model on model predictions, iii) inclusion separation to the ladle wall, and iv) the separation of inclusions to the slag would be

of interest to carry out. Such studies would increase the fundamental knowledge regarding micro-inclusion behavior in gas-stirred ladles. Static and dynamic modeling results could then begin to be used in the development of equations for process control models of inclusion growth and removal.

REFERENCES

1. Reinholdsson F., Lind A., Nilsson R. and Jönsson P., Proceedings Clean Steel 5, vol 2, Balatonfured, Hungary, June 1997, pp. 96-106, 1999
2. Reinholdsson F., Lind A., Nilsson R., Sjödin P. and Jönsson P.G., ISIJ International vol 37 (1997) no 6, pp. 637-639
3. Lindborg U. and Torssell K. Trans. Met. Soc. AIME, vol 242 (1968), pp. 94 - 102.
4. Iyengar R.K. and Philibrook W.O. Met. Trans., vol. 3 (1972), pp. 1823-1830.
5. Linder S., Scandinavian Journal of Metallurgy. 3 (1974) 137-150
6. Engh T.A. and Lindskog N., Scandinavian Journal of Metallurgy vol. 4 (1975) no. 2 pp 49-58
7. Nakanishi K. and Szekely J., Trans. ISIJ, vol 15 (1975) pp. 522-530
8. Saffman P.G. and Turner J.S. J. Fluid Mch., vol. 1 (1956), pp. 16-30
9. Shirabe K. and Szekely J., ISIJ International, vol. 23 (1983) pp. 465-474
10. Johansen S.T., Boysan F. and Engh T.A., Procceedings Fourth Japan-Nordic Countries Joint Symposium on Science and Technology of Process Metallurgy, Tokyo, Japan, November 1986, pp 182-215
11. Tacke K-H. and Ludwig J.C., Steel Research vol 58 (1987) no6, pp. 262-270
12. Ilegbusi O.J. and Szekely J., ISIJ International, vol 29 (1989), no 12, pp. 1031-1039
13. Kaufmann B., Niedermeyr A., Sattler H. and Preuer A., Steel Research vol 64 (1993) no 4, pp. 203-209
14. Sinha A.K. and Sahai Y., ISIJ International, vol 33 (1993), no5 pp. 556-566
15. Joo S., Han J.W. and Guthrie R.I.L., Metallurgical Transactions B (USA), vol. 24B (1993), no. 5, pp. 767-777
16. Hallberg M., Tech. lic. Thesis, Royal Institute of Technology, Sweden (1996)
17. Miki Y., Shimada Y., Thomas B.G. and Denisov A., I&SM, ISS vol 28 (1997) pp. 31-38
18. Wakoh M., Fuchigami K., Endoh K., Imamura N., Kiyose A. and Sawada I., Scanmet I, Luleå, Sweden, June, 1999, pp. 267-274
19. Miki Y. and Thomas B.G., Metallurgical and Materials Transactions B, vol 30B (1999) pp. 639-654
20. Tozawa H., Kato Y., Sorimachi K. and Nakanishi T., ISIJ International, vol 39 (1999) no 5, pp. 426-434
21. Swedish Standard SS 11 11 16, Swedish Institute for Standards, SIS Tryckeri, Stockholm, Sweden, (1985)
22. Higashitani K., Yamauchi K., Matsuno Y. and Hosokawa G., Chem. Eng. Jpn., vol 16 (1983) no. 4, pp. 299-304.
23. Taniguchi S., Kikuchi A., Ise T. and Shoji N. ISIJ International, vol 36 (1996), Suplement, pp. S117-S120
24. Taniguchi S. and Kikuchi A., Tetsu-to-hagane, vol. 78 (1992), pp. 527-535.
25. Wang L., Lee H-G. and Hayes P., ISIJ International, vol. 36 (1996) no 1 pp. 7-16

26. Yoon R.H. and Lutrell G.H., Mineral Proess. and Extractice Metall. Rev., vol 4 (1989) pp. 101-122
27. Schulze H.J., Miner. Process. Extrac. Metall. Rev. vol 5 (1989) pp. 43-76
28. Frisvold F., Engh T.A., Johansen S.T. and Pedersen T. Light Metals 1992, San Diego, California, USA, March 1992, The Minerals, Metals & Materials Society (USA), pp. 1125-1132
29. Engh T. A. Principles of metal refining. Oxford university press. (1992) ISBN 0-19-856337-X
30. Jonsson L., S. Du and Jönsson P.G. ISIJ International, vol. 38 (1998) no.3 pp. 260-267
31. Jönsson P.G. and Jonsson L., Scandinavian Journal of Metallurgy, vol. 24 (1995) pp. 194-206
32. Spalding, D. B et. al., Phoenics Encyclopedia, 1997, CHAM
33. Launder B. E. And Spalding D. B., Computer Methods in Aren;t Mechanics and Eng., vol.3 (1974), pp.269-289
34. Andrews M. J., Ph.D thesis, Imperial College, 1996
35. Spalding D. B.: Recent Advaces in Numercial Method in Fluid, ed. By Taylor C. And Morgan K., Pineridge Press, Swansea, England, pp.139

Table I. Possibilities to control steel quality parameters during steelmaking.

	Ladle	Tundish	Mold	Metal working mill
Elements that dissolve in steel	yes	yes	yes	yes, not necessary
Temperature	yes	yes	yes	yes
Micro and macro inclusions	no	no	no	yes, afterwards

Table II. Summarizing table over CFD models considering inclusion growth and/or removal.

Referens						**Growth**				**Removal**					**Reox**				
	Year	Turbulence model	Heat flow	Dimension	Sep. fl/incl model	Turbulent	Stoke	Laminar	Brown	Stoke/buoyancy	Gas bubble	To slag *	To refractory	Dispersion of slag	Slag	Refractory	Vessel	Stirring	Other
Nakanishi & Szekely	1975	2Eq	N	2D	sep	Y	N	N	N	N	N	N	N	N	N	N	ladle	ind.	**
Shirabe & Szekely	1983	k-ε	N	2D	sep	Y	N	N	N	Y	N	N	N	N	N	N	RH	(gas)	
Johansen et al	1986	k-ε	N	2D	sep	N	N	N	N	Y	N	Y	Y	N	N	Y	ladle	gas	
Tacke & Ludwig	1987	k-ε	N	3D	int	N	N	N	N	Y	N	N	N	N	N	N	tund	no	
Ilegbusi & Szekely	1989	k-ε	Y	3D	int	Y	N	N	N	Y	N	N	N	N	N	N	tund	no	
Kaufmann et al	1993	k-ε	N	3D	-	N	N	N	N	Y	N	N	N	N	N	N	tund	no	+
Sinha & Sahai	1993	k-ε	N	3D	sep	Y	N	N	N	Y	N	N	Y	N	N	N	tund	no	
Joo, Han & Guthrie	1993	k-ε	Y	3D	int	N	N	N	N	Y	N	N	N	N	N	N	tund	no	
Hallberg	1996	k-ε	N	3D	sep	Y	Y	N	N	Y	N	N	Y	N	Y	N	ladle	gas/ind	
Miki et al	1997	k-ε	N	3D	sep	Y	Y	N	N	Y	Y	N	N	N	N	N	RH	(gas)	++
Wakoh et al	1999	k-ε	N	3D	sep	Y	Y	N	Y	Y	Y	N	N	Y	N	N	ladle	gas	
Miki & Thomas	1999	k-ε	Y	3D	sep	Y	Y	N	N	Y	N	N	N	N	N	N	tund	no	++
Tozawa et al	1999	k-ε	Y	3D	int	Y	Y	N	Y	Y	N	N	N	N	N	N	tund	no	++

N = no, Y = yes
* = removal to slag by turbulent diffusion
** = inclusions over a certain size was considered floated out.
$^{+}$ = no inclusion model calculated in the model
$^{++}$ = considering cluster formation

Table III. Classification of inclusion intervals and inclusion density used as initial conditions in the simulations.

Classification	Size interval (μm)	Number of inclusions/m^3
DT	2.8-5.6	$2.328x10^{10}$
DM	5.6-11.2	$3.106x10^{9}$
DH	11.2-22.4	$2.360x10^{8}$

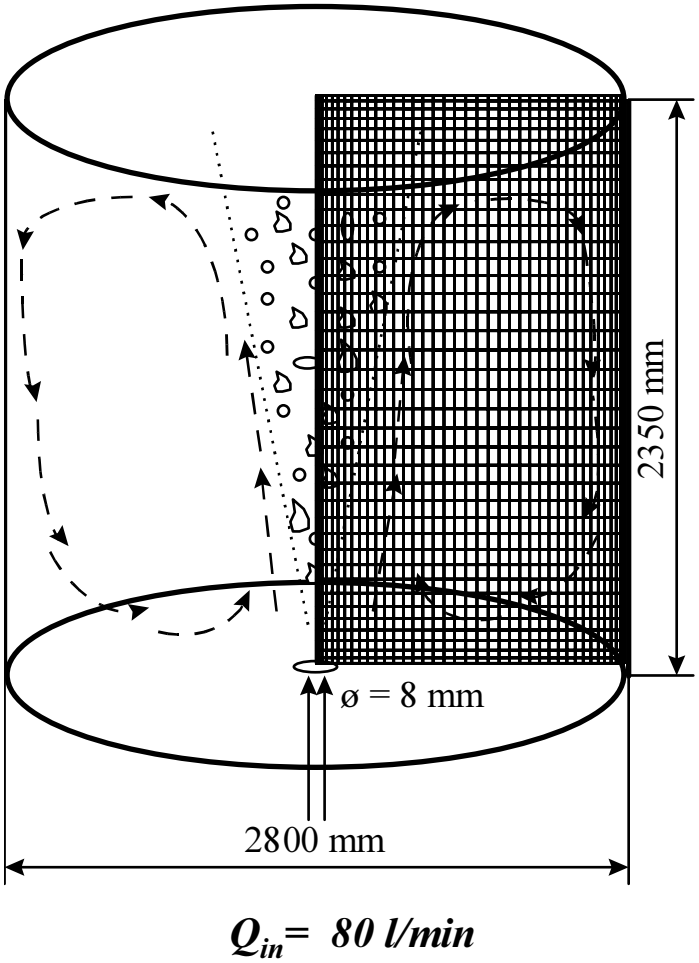

Figure 1: Schematic sketch and grid distribution (31*40) of gas-stirred ladle.

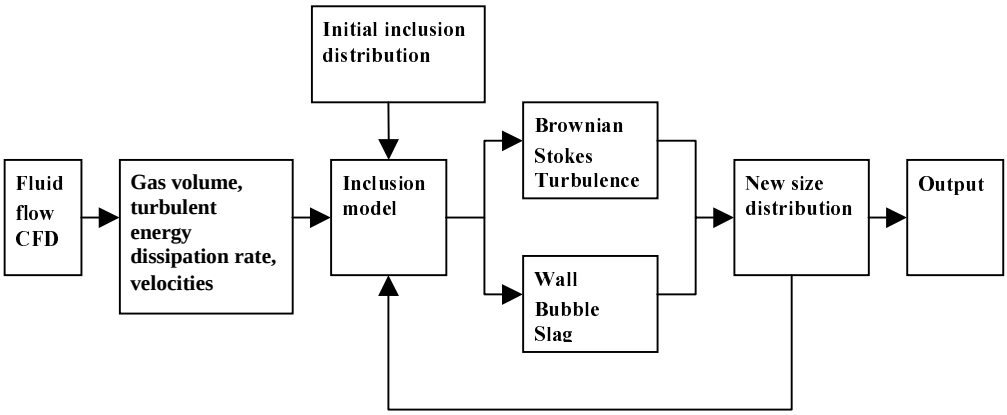

Figure 2: Flow chart of the mathematical model.

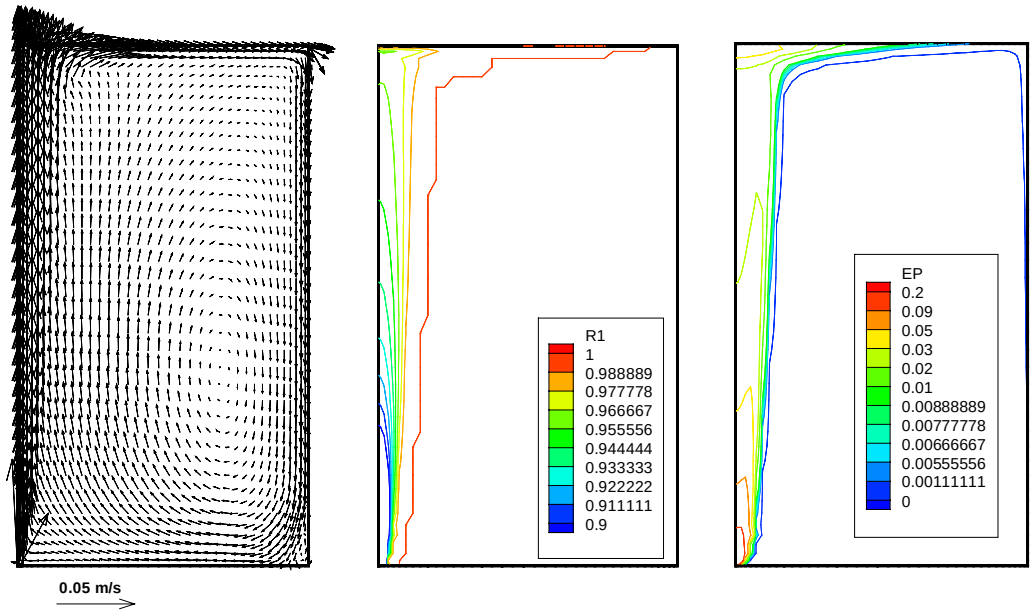

(a) Flow pattern (b) liquid volume fraction (c) ε distribution

Figure 3: Simulation results of the fluid flow model in the gas stirred ladle.

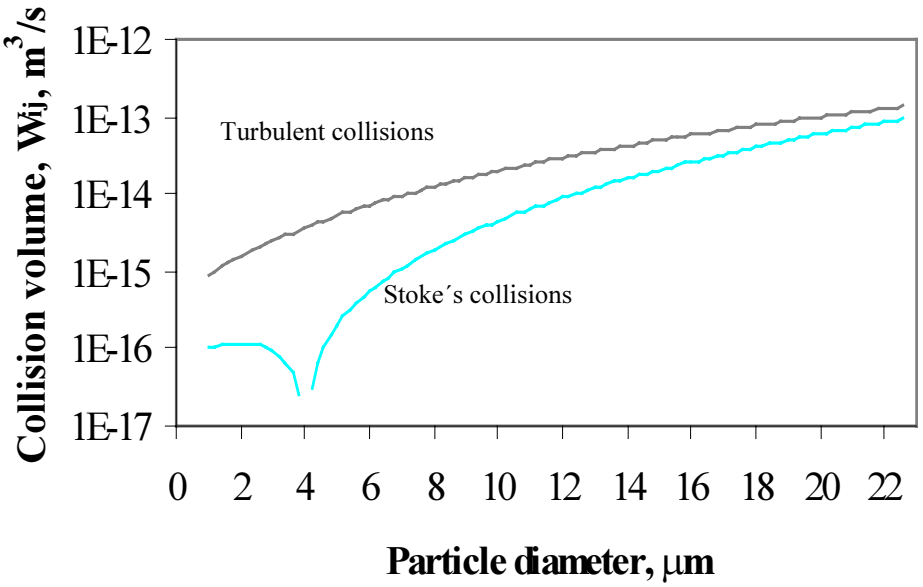

Figure 4: Collision volume for an inclusion with a 2 μm radius as a function of the other inclusion's radius.

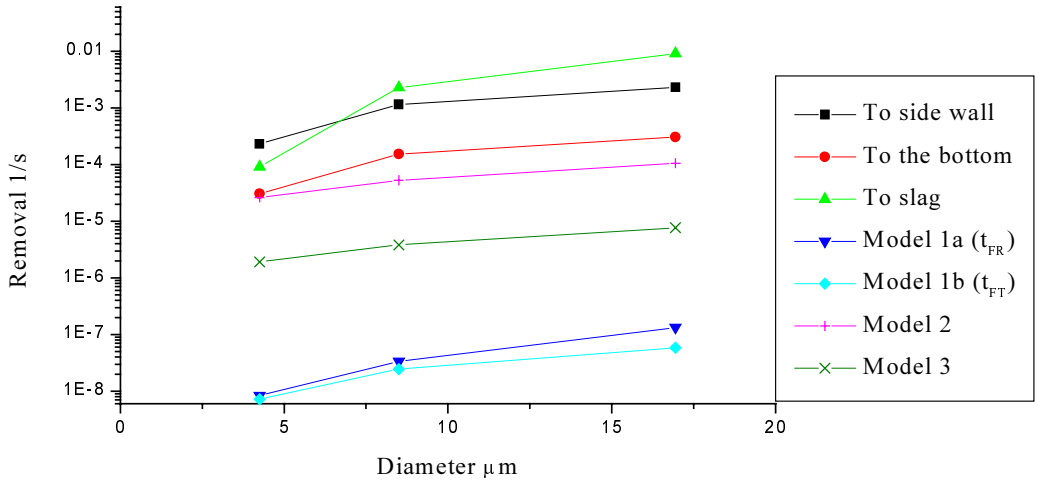

Figure 5: Comparison of inclusion removal rate for different mechanisms.

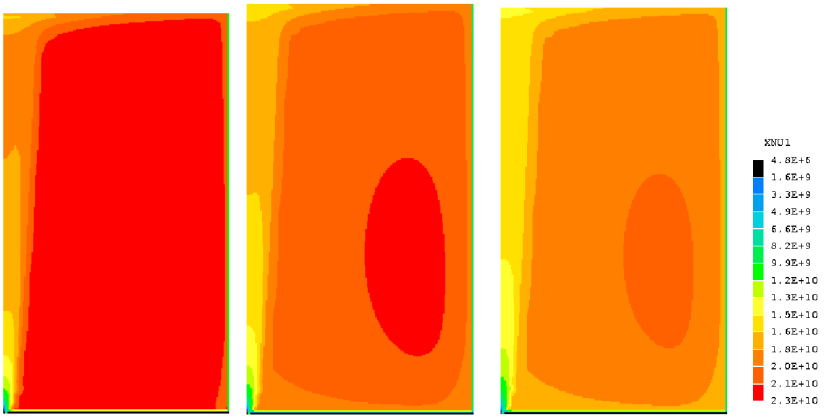

t=60s, t=180s, t=300s

(a) GroupA 2.8-5.6um

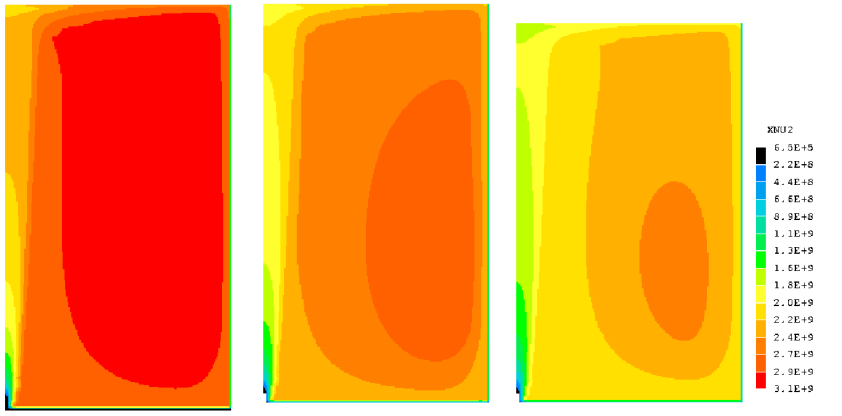

t=60s, t=180s, t=300s

(b) GroupB 5.6-11.2um

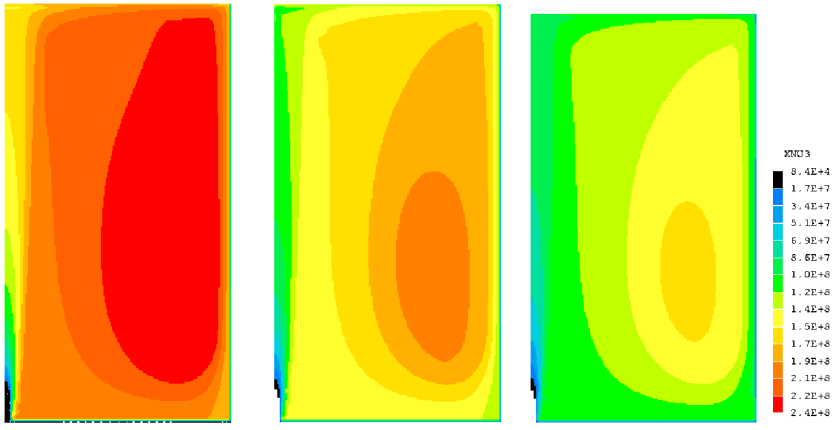

t=60s, t=180s, t=300s

(c) GroupC 11.2-22.4 um

Figure 6: Transient contour plots of the inclusion particles density

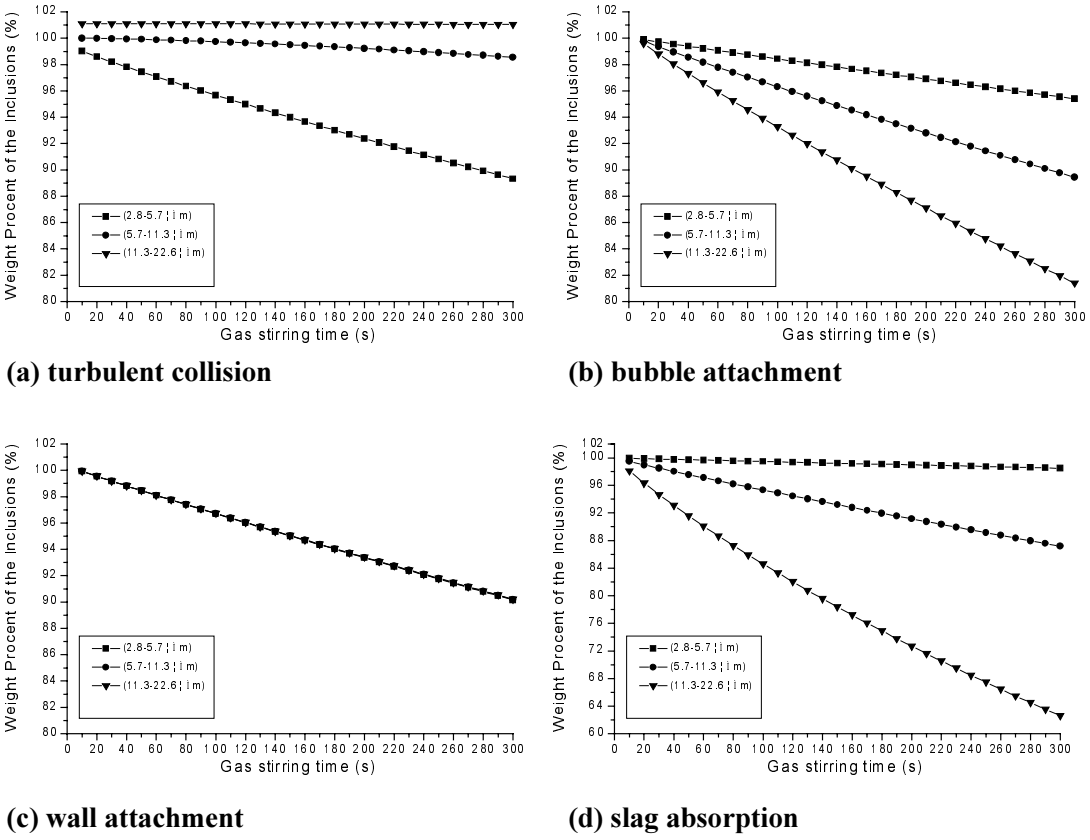

Figure 7: Comparison of transient inclusion weight fraction due to different (isolated) removal mechanisms

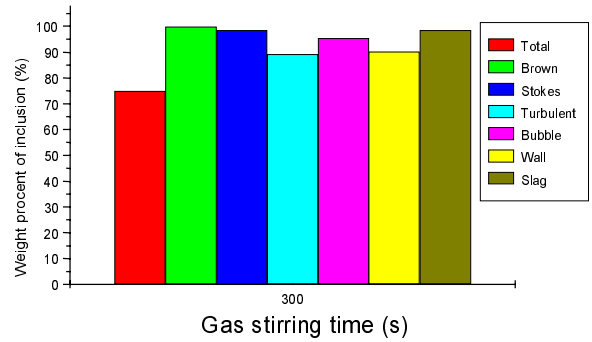

(a) Group A, 2.8-5.7 μm

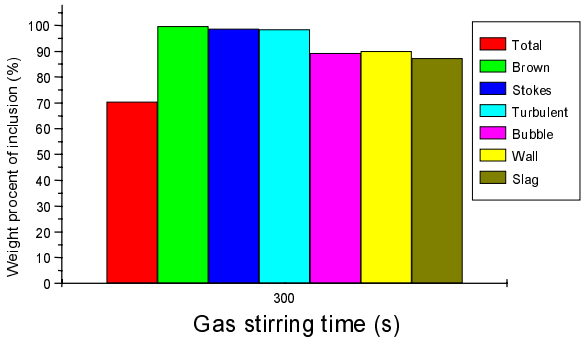

(b) Group B, 5.7-11.3 μm

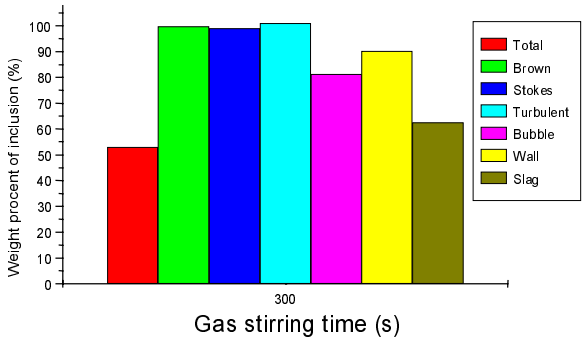

(c) Group C, 11.3-22.6 μm

Figure 8: Inclusion weight fraction after 5 minutes gas stirring due to different (isolated) growth and removal mechanisms